Taylor & Francis
Taylor & Francis Group

Interplay between radiation pressure force and scattered light intensity in the cooperative scattering by cold atoms

T. Bienaimé[a], R. Bachelard[b], J. Chabé[a], M.T. Rouabah[a,c], L. Bellando[a], Ph.W. Courteille[b], N. Piovella[d] and R. Kaiser[a]*

[a] *Université de Nice Sophia Antipolis, CNRS, Institut Non-Linéaire de Nice, UMR 7335, F-06560 Valbonne, France;* [b] *Instituto de Física de São Carlos, Universidade de São Paulo, 13560-970 São Carlos, SP, Brazil;* [c] *Laboratoire de Physique Mathématique et Physique Subatomique, Université Constantine 1, Constantine 25000, Algeria;* [d] *Dipartimento di Fisica, Università Degli Studi di Milano, Via Celoria 16, I-20133 Milano, Italy*

The interplay between the superradiant emission of a cloud of cold two-level atoms and the radiation pressure force is discussed. Using a microscopic model of coupled atomic dipoles driven by an external laser, the radiation field and the average radiation pressure force are derived. A relation between the far-field scattered intensity and the force is derived, using the optical theorem. Finally, the scaling of the sample scattering cross-section with the parameters of the system is studied.

Keywords: cold atoms; Dicke superradiance; cooperative scattering

1. Introduction

Cooperative effects occur when the behavior of a many body system is determined by their collective interactions with each other and thus manifest themselves in a large variety of physical systems. In this paper, we focus on the specific case of a collection of atoms illuminated by a laser. In this situation, the electro-magnetic field mediates resonant dipole–dipole interactions between the atoms, leading to a cooperative response of the system, which quantitatively differs from the single atom response. Such effects are imprinted on physical observables that can be experimentally measured such as e.g. the emission diagram or the radiation pressure force acting on the cloud.

When a single atom is illuminated by a laser, the scattering process results in a force proportional to the number of scattered photons. Indeed, as an atom absorbs a photon from the laser of wave vector $\mathbf{k}_0$, it acquires a momentum $\hbar\mathbf{k}_0$, but the average momentum change during the emission process is zero.

For a collection of atoms, the picture changes drastically as it was first noticed in a pioneering work by Dicke [1] where he showed enhanced spontaneous emission decay rates in small and large samples due to constructive interferences of collective emission. In the situation of an incident laser scattering on a cloud of atoms, the atoms cooperate to scatter the light leading to a directional emission. This phenomenon is due to the synchronization of the atomic dipoles with the laser. The collective effects become even

stronger as the atomic medium becomes optically dense and the radiation of the atoms starts to alter significantly the wave propagation. Among the other collective effects that arise, one can mention the collective Lamb shift [2,3], Mie resonances [4], subradiance [5], the refractive index of a dilute Bose gas [6] as well as a reduction of the radiation pressure force [7,8].

Since the radiated light results from the interference of the waves emitted by each dipole, the simple relation between emitted photon and atomic recoil is lost. For example, a striking feature of cooperativity is the modification of the atomic recoil due to the presence of the neighboring atoms [9,10], an effect that cannot be deduced from single-atom physics.

We here discuss the particular relation between the directional superradiant emission, and the reduction of the radiation pressure force. The atomic cloud is described as a microscopic ensemble of coupled atomic dipoles, and both the radiated field and the force are expressed as a function of these dipoles. The optical theorem is derived in this framework, and is shown to lead to a direct relation between intensity scattered and radiation pressure force for the cloud center-of-mass.

2. Cooperative scattering model

The atomic cloud is described as a system of two-level (*g* and *e*) atoms, with resonant frequency ω_a and position

---

*Corresponding author. Email: robin.kaiser@inln.cnrs.fr

$\mathbf{r}_j$, that are driven by an uniform laser beam with electric field amplitude E_0, frequency ω_0 and wave vector $\mathbf{k}_0 = (\omega_0/c)\hat{\mathbf{e}}_z$. The laser–atom interaction is described by the following Hamiltonian:

$$H = \frac{\hbar\Omega_0}{2} \sum_{j=1}^{N} \left[\hat{\sigma}_j \exp[i(\Delta_0 t - \mathbf{k}_0 \cdot \mathbf{r}_j)] + \text{h.c.} \right]$$
$$+ \hbar \sum_{j=1}^{N} \sum_{\mathbf{k}} g_k \left(\hat{\sigma}_j \exp(-i\omega_a t) + \hat{\sigma}_j^\dagger \exp(i\omega_a t) \right)$$
$$\times \left[\hat{a}_{\mathbf{k}}^\dagger \exp[i(\omega_k t - \mathbf{k} \cdot \mathbf{r}_j)] + \hat{a}_{\mathbf{k}} \exp[-i(\omega_k t - \mathbf{k} \cdot \mathbf{r}_j)] \right], \quad (1)$$

where $\Omega_0 = dE_0/\hbar$ is the Rabi frequency of the incident laser field and $\Delta_0 = \omega_0 - \omega_a$ is the detuning between the laser and the atomic transition. In Equation (1) $\hat{\sigma}_j = |g_j\rangle\langle e_j|$ is the lowering operator for the j-atom, $\hat{a}_{\mathbf{k}}$ is the photon annihilation operator and $g_k = (d^2\omega_k/2\hbar\epsilon_0 V)^{1/2}$ is the single-photon Rabi frequency, where d is the electric-dipole transition matrix element and V is the photon mode volume. The special case where a single photon (mode $\mathbf{k}$) can be assumed to be present in the system, was extensively investigated in [2,11,12], and later extended to include a low-intensity laser in [7,13,14]. The system atoms+photons is then described by a state of the form [15]:

$$|\Psi\rangle = \alpha(t)|g_1 \ldots g_N\rangle|0\rangle_{\mathbf{k}}$$
$$+ \exp(-i\Delta_0 t) \sum_{j=1}^{N} \beta_j(t)|g_1 \ldots e_j \ldots g_N\rangle|0\rangle_{\mathbf{k}}$$
$$+ \sum_{\mathbf{k}} \gamma_{\mathbf{k}}(t)|g_1 \ldots g_N\rangle|1\rangle_{\mathbf{k}}$$
$$+ \sum_{\mathbf{k}} \sum_{m,n=1}^{N} \epsilon_{m<n,\mathbf{k}}(t)|g_1 \ldots e_m \ldots e_n \ldots g_N\rangle|1\rangle_{\mathbf{k}}, \quad (2)$$

The first term in Equation (2) corresponds to the initial ground state without photons, the second term is the sum over the states where a single atom has been excited by the classical field. The third term corresponds to the atoms that returned to the ground state having emitted a photon in the mode $\mathbf{k}$, whereas the last one corresponds to the presence of two excited atoms and one virtual photon with 'negative' energy. It is due to the counter-rotating terms in Hamiltonian (1) and this disappears when the rotating wave approximation is made. In the linear regime $\alpha \approx 1$ and in the Markov approximation, valid if the decay time is larger than the photon time-of-flight through the atomic cloud, the scattering problem reduces to the following differential equation [13,14,16]

$$\dot{\beta}_j = \left(i\Delta_0 - \frac{\Gamma}{2} \right) \beta_j - i\frac{\Omega_0}{2} \exp(i\mathbf{k}_0 \cdot \mathbf{r}_j)$$
$$- \frac{\Gamma}{2} \sum_{m \neq j} \frac{\exp(ik_0|\mathbf{r}_j - \mathbf{r}_m|)}{ik_0|\mathbf{r}_j - \mathbf{r}_m|} \beta_m \quad (3)$$

with initial condition $\beta_j(0) = 0$, for $j = 1, \ldots, N$. Here, $\Gamma = Vg_k^2 k_0^2/\pi c = d^2 k_0^3/2\pi\epsilon_0\hbar$ is the single-atom *spontaneous* decay rate. The kernel in the last term of Equation (3) has a real component, $-(\Gamma/2)\sum_{m\neq j}[\sin(x_{jm})/x_{jm}]$ (where $x_{jm} = k_0|\mathbf{r}_j - \mathbf{r}_m|$), describing the *collective* atomic decay, and an imaginary component, $i(\Gamma/2)\sum_{m\neq j}[\cos(x_{jm})/x_{jm}]$, describing the collective Lamb shift [16–18]. Notice that while Equation (3) is here deduced from a quantum mechanical model, it can also be obtained classically, treating the two-level atoms as weakly excited classical harmonic oscillators [15,19].

3. Radiated field

The radiation field operator $\hat{a}_{\mathbf{k}}$ evolves according to the following Heisenberg equation

$$\frac{d\hat{a}_{\mathbf{k}}}{dt} = \frac{1}{i\hbar}[\hat{a}_{\mathbf{k}}, \hat{H}]$$
$$= -ig_k \exp[i(\omega_k - \omega_a)t] \sum_{m=1}^{N} \hat{\sigma}_m \exp(-i\mathbf{k} \cdot \mathbf{r}_m), \quad (4)$$

where the fast oscillating term proportional to $\exp[i(\omega_k + \omega_a)t]$ has been neglected. The scattered field is obtained by performing the sum over all the modes, considering only the positive-frequency part of the electric field operator

$$\hat{E}_s(\mathbf{r}, t) = \sum_{\mathbf{k}} \mathcal{E}_k \hat{a}_{\mathbf{k}}(t) \exp(i\mathbf{k} \cdot \mathbf{r} - i\omega_k t), \quad (5)$$

where $\mathcal{E}_k = (\hbar\omega_k/2\epsilon_0 V)^{1/2}$. Integrating Equation (4) with respect to time, with $a_{\mathbf{k}}(0) = 0$, inserting it in Equation (5), and assuming the usual Markov approximation, one obtains [14]

$$\hat{E}_s(\mathbf{r}, t) \approx -\frac{dk_0^3}{4\pi\epsilon_0} \exp(-i\omega_a t) \sum_{m=1}^{N} \frac{\exp(ik_0|\mathbf{r} - \mathbf{r}_m|)}{k_0|\mathbf{r} - \mathbf{r}_m|} \hat{\sigma}_m(t). \quad (6)$$

When applied on the state (2), neglecting virtual transitions, it yields $\hat{E}_s|\Psi\rangle = E_s \exp(-i\omega_0 t)|g_1 \ldots g_N\rangle$, with

$$E_s(\mathbf{r}, t) = -\frac{\hbar\Gamma}{2d} \sum_{m=1}^{N} \beta_m(t) \frac{\exp(ik_0|\mathbf{r} - \mathbf{r}_m|)}{k_0|\mathbf{r} - \mathbf{r}_m|}. \quad (7)$$

Hence, the radiated field appears as a sum of spherical waves radiated by the atomic dipoles. In the far-field limit, one has $k_0|\mathbf{r} - \mathbf{r}_m| \approx k_0 r - \mathbf{k} \cdot \mathbf{r}_m$, with $\mathbf{k} = k_0(\mathbf{r}/r)$, so the field (7) radiated in a direction $\mathbf{k}$ reads

$$E_s^{(\text{far})}(\mathbf{k}, t) \approx -\frac{\hbar\Gamma}{2d} \frac{\exp(ik_0 r)}{k_0 r} \sum_{m=1}^{N} \beta_m(t) \exp(-i\mathbf{k} \cdot \mathbf{r}_m). \quad (8)$$

The scattered intensity in a direction $\mathbf{k}$ is then derived as

$$I_s(\mathbf{k}) = \frac{\epsilon_0 c \hbar^2 \Gamma^2}{2(dk_0 r)^2} \left| \sum_{m=1}^{N} \beta_m(t) \exp(-i\mathbf{k} \cdot \mathbf{r}_m) \right|^2 \tag{9}$$

$$= \frac{\epsilon_0 c \hbar^2 \Gamma^2}{2(dk_0 r)^2}$$
$$\times \left(\sum_{m=1}^{N} |\beta_m|^2 + \sum_{j \neq m}^{N} \beta_j \beta_m^* \exp[-i\mathbf{k} \cdot (\mathbf{r}_j - \mathbf{r}_m)] \right). \tag{10}$$

Integrating this intensity over all directions leads to the total scattered power

$$P_r = \frac{d^2 k_0^4 c}{2\pi \epsilon_0} \left(\sum_{m=1}^{N} |\beta_m|^2 + \sum_{m \neq j}^{N} \beta_j \beta_m^* \frac{\sin(k_0 |\mathbf{r}_j - \mathbf{r}_m|)}{k_0 |\mathbf{r}_j - \mathbf{r}_m|} \right), \tag{11}$$

where we have used the equality

$$\int d\hat{\mathbf{k}} e^{ik_0 \hat{\mathbf{k}} \cdot \mathbf{d}} = 4\pi \frac{\sin(k_0|d|)}{k_0|d|}. \tag{12}$$

In Equation (11), the first term corresponds to the *incoherent* sum of the single atom radiated power. The second term is an interference term; in the limit of a cloud small compared to the wavelength, the dipole moments have the same phase and this latter term is responsible for a superradiant build-up of the radiated power $\propto N^2$ (see, e.g. [1]).

4. Radiation pressure force

As for the radiation force operator acting on the jth atom, it is derived from Equation (1) as

$$\hat{\mathbf{F}}_j = -\nabla_{\mathbf{r}_j} \hat{H} = \hat{\mathbf{F}}_{aj} + \hat{\mathbf{F}}_{ej}. \tag{13}$$

A first contribution associated with the absorption of photons of the pump appears [7,13]:

$$\hat{\mathbf{F}}_{aj} = i\hbar\mathbf{k}_0 \frac{\Omega_0}{2} \left\{ \hat{\sigma}_j \exp[i(\Delta_0 t - \mathbf{k}_0 \cdot \mathbf{r}_j)] - \text{h.c.} \right\}, \tag{14}$$

whereas the second contribution comes from the emission of the photons in any direction $\mathbf{k}$:

$$\hat{\mathbf{F}}_{ej} = i\hbar \sum_{\mathbf{k}} \mathbf{k} g_k \left\{ \hat{a}_{\mathbf{k}}^{\dagger} \hat{\sigma}_j \exp[i(\omega_k - \omega_a)t - i\mathbf{k} \cdot \mathbf{r}_j] \right.$$
$$\left. - \hat{\sigma}_j^{\dagger} \hat{a}_{\mathbf{k}} \exp[-i(\omega_k - \omega_a)t + i\mathbf{k} \cdot \mathbf{r}_j] \right\}. \tag{15}$$

In Equation (15), the counter-rotating terms proportional to $\exp[\pm i(\omega_k + \omega_a)t]$ were neglected.

As we are interested in comparing the radiation pressure force to the single-atom case, we define the average radiation force $\hat{\mathbf{F}} = (1/N) \sum_j \hat{\mathbf{F}}_j = (F_{\text{tot}}/N)\hat{\mathbf{e}}_z$ that measures acceleration of the cloud center-of-mass given by $\mathbf{a}_{\text{CM}} = \hat{\mathbf{F}}/m$, with m the single-atom mass. Note that this average force is N times smaller than the total force F_{tot} acting on the whole cloud of atoms. Since we consider clouds

with rotational symmetry around the laser axis, this force is in the same direction as the incident field wave vector $\mathbf{k}_0 = k_0 \hat{\mathbf{e}}_z$. This average force is measured by time-of-flight techniques in cold atomic clouds released, for instance, from magneto-optical traps (MOTs) and has recently revealed cooperative effects in the scattering by extended atomic samples [8,20]. Like the scattered radiation, this force is an observable that contains signatures of the cooperative scattering by the atoms [7,8]. The average absorption force along the z-axis, resulting from the recoil received upon absorption of a photon from the incident laser, reads

$$\hat{F}_a = \frac{i}{2N} \hbar k_0 \Omega_0 \sum_{j=1}^{N} \left[\hat{\sigma}_j \exp(i\Delta_0 t - i\mathbf{k}_0 \cdot \mathbf{r}_j) - \text{h.c.} \right]. \tag{16}$$

Similarly, the average emission force writes $\hat{\mathbf{F}}_e = (1/N) \sum_j \hat{\mathbf{F}}_{ej}$. Inserting the expression for $\hat{a}_{\mathbf{k}}$ from Equation (4) into Equation (15), and approximating the discrete sum over the modes $\mathbf{k}$ by an integral, it is possible to obtain, as was done for the radiation field operator $\hat{E}_S$ of Equation (7), the following expression for the average emission force along the z-axis [7]:

$$\hat{F}_e = -\frac{\hbar k_0 \Gamma}{8\pi N} \int_0^{2\pi} d\phi \int_0^{\pi} d\theta \sin\theta \cos\theta$$
$$\times \sum_{j,m=1}^{N} \left[\exp[-i\mathbf{k} \cdot (\mathbf{r}_j - \mathbf{r}_m)] \hat{\sigma}_m^{\dagger} \hat{\sigma}_j + \text{h.c.} \right]. \tag{17}$$

Neglecting virtual photon contributions, the expectation values of the absorption and emission forces for state (2) are

$$\langle \hat{F}_a \rangle = -\frac{\hbar k_0 \Omega_0}{N} \sum_{j=1}^{N} \text{Im} \left[\beta_j \exp(-i\mathbf{k}_0 \cdot \mathbf{r}_j) \right], \tag{18}$$

$$\langle \hat{F}_e \rangle = -\frac{\hbar k_0 \Gamma}{4\pi N} \int_0^{2\pi} d\phi \int_0^{\pi} d\theta \sin\theta \cos\theta$$
$$\times \sum_{j,m=1}^{N} \left(\beta_j \beta_m^* \exp[-i\mathbf{k} \cdot (\mathbf{r}_j - \mathbf{r}_m)] \right)$$
$$= -\frac{\hbar k_0 \Gamma}{N} \sum_{j,m=1}^{N} \frac{(z_j - z_m)}{|\mathbf{r}_j - \mathbf{r}_m|} j_1(k_0|\mathbf{r}_j - \mathbf{r}_m|) \text{Im} \left(\beta_j \beta_m^* \right), \tag{19}$$

where we used the identity

$$\int_0^{2\pi} d\phi \int_0^{\pi} d\theta \sin\theta \cos\theta \exp[-i\mathbf{k} \cdot (\mathbf{r} - \mathbf{r}')]$$
$$= 4\pi i \frac{z - z'}{|\mathbf{r} - \mathbf{r}'|} j_1(k_0|\mathbf{r} - \mathbf{r}'|). \tag{20}$$

$j_1(z)$ here refers the first-order spherical Bessel function. Note that the decomposition into absorption (18) and emission (19) forces is fully compatible with classical expressions of the optical force [21], where the force arises as the product between the atomic dipole and the *total* field [22] (i.e. including the radiation from the other atoms).

5. Optical theorem

Let us now discuss the formulation of the optical theorem in the framework of collective scattering. To that purpose, we consider an infinite slab illuminated by a plane wave. In the far-field limit, the field in a direction $\hat{\mathbf{k}}$ is

$$
\begin{aligned}
E(\mathbf{r}) &= \left[\frac{E_0}{2} \exp(ik_0 z) + E_s^{(\mathrm{far})}(r, \hat{\mathbf{k}}) \right] \exp(-i\omega_0 t) \\
&= \frac{E_0}{2} \left[\exp(ik_0 z) - \frac{\exp(ik_0 r)}{k_0 r} f(\hat{\mathbf{k}}) \right] \exp(-i\omega_0 t),
\end{aligned}
\tag{21}
$$

where the scattering amplitude for the scattered field f is given by

$$
f(\hat{\mathbf{k}}) = \frac{\Gamma}{\Omega_0} \sum_j \beta_j \exp(-ik_0 \hat{\mathbf{k}} \cdot \mathbf{r}_j).
\tag{22}
$$

As a consequence, the scattered intensity at a large distance r from the cloud is

$$
I_s = I_0 \frac{|f(\hat{\mathbf{k}})|^2}{k_0^2 r^2},
\tag{23}
$$

while the total scattering cross-section is obtained by integrating over all the solid angle

$$
\sigma_{\mathrm{sca}} = \frac{1}{k_0^2} \int d\hat{\mathbf{k}} |f(\hat{\mathbf{k}})|^2.
\tag{24}
$$

To simulate numerically the slab illuminated by a plane wave, we consider a cylinder of transverse size large
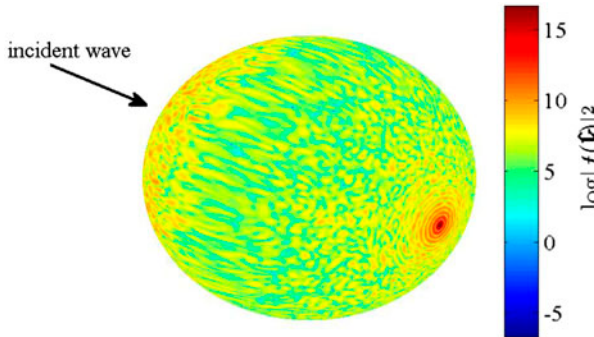

Figure 1. Scattering amplitude $|f(\hat{\mathbf{k}})|^2$ as given by Equation (22) for a cylindrical cloud of thickness $30/k_0$ and radius $90/k_0$, illuminated by a plane wave. The direction of the incoming wave is indicated by an arrow. The number of scatterers is $N = 20{,}000$, the detuning $\Delta_0 = 0$. The color-coded intensity is represented in log-scale. One can clearly see in red the strong forward emission of the sample, reminiscent of Mie scattering by large clouds compared to the wavelength. In the other directions, the scattered field is speckle-like due to the randomly positioned two-level scatterers, and describes the spontaneous emission by the cloud. Performing configuration averages would smooth out these fluctuations, except in the backward direction where, in the multiple scattering regime, the well-known coherent backscattering cone is recovered [23,24]. Finally, the emission in the transverse dimension is reduced due to the quasi-one-dimensional geometry. (The color version of this figure is included in the online version of the journal.)

compared to its thickness and to the wavelength, with a random homogeneous distribution of atoms. Figure 1 shows the emission diagram of the scattered field for resonant excitation and a cylindrical cloud of atoms. The energy conservation imposes that

$$
\sigma_{\mathrm{ext}} = \sigma_{\mathrm{sca}} + \sigma_{\mathrm{abs}},
\tag{25}
$$

where σ_{ext} and σ_{abs} are the cross-sections for extinction and absorption, respectively. The extinction cross-section is then obtained from the optical theorem. In the forward direction the total field is

$$
E_{\mathrm{fwd}}(\theta = 0) = \frac{E_0}{2} \left[\exp(ik_0 z) - \frac{\exp(ik_0 r)}{k_0 r} f(0) \right] \exp(-i\omega_0 t).
\tag{26}
$$

In the slab configuration, the cloud radiates mainly in a narrow forward cone – the angle of the cone of emission is given by the inverse of the cloud transverse size. Hence, observing the field in a plane far from the atoms and within the forward cone of emission, the radius expands as $r \approx z + (x^2 + y^2)/2z$, and one obtains

$$
\begin{aligned}
E_{\mathrm{fwd}}(\mathbf{r}) \approx \frac{E_0}{2} &\left[1 - \frac{f(0)}{k_0 z} \exp[ik_0(x^2 + y^2)/2z] \right] \\
&\times \exp[i(k_0 z - \omega_0 t)].
\end{aligned}
\tag{27}
$$

So the intensity reads

$$
|E_{\mathrm{fwd}}(\mathbf{r})|^2 \approx \frac{|E_0|^2}{4} \left\{ 1 - \frac{2}{k_0 z} \mathrm{Re} \left[f(0) \exp[ik(x^2 + y^2)/2z] \right] \right\},
\tag{28}
$$

since we have neglected the quadratic term $|E_s|^2$. The measured intensity is the incident intensity minus the extinction intensity. In Equation (28), the integration over x, y yields a factor $2i\pi z/k_0$, and one gets

$$
\sigma_{\mathrm{ext}} = -\frac{4\pi}{k_0^2} \mathrm{Im}[f(0)].
\tag{29}
$$

Hence, from Equation (24) one obtains the relation

$$
-\mathrm{Im}[f(0)] = \frac{1}{4\pi} \int d\hat{\mathbf{k}} |f(\hat{\mathbf{k}})|^2 + \frac{k_0^2}{4\pi} \sigma_{\mathrm{abs}}.
\tag{30}
$$

In our microscopic description of the light–atom interaction there is no absorption, so that $\sigma_{\mathrm{abs}} = 0$. An illustration of the validity of the optical theorem is given in Figure 2 for resonant light scattering by a slab containing two-level scatterers with a uniform density distribution. From Equations (22) and (29), and introducing the wavevector $\mathbf{k} = k_0 \hat{\mathbf{k}}(\theta, \phi)$, we obtain the relation

$$
\begin{aligned}
&-\frac{\Omega_0}{\Gamma} \sum_j \mathrm{Im} \left[\beta_j \exp(-i\mathbf{k}_0 \cdot \mathbf{r}_j) \right] \\
&= \frac{1}{4\pi} \int_0^{2\pi} d\phi \int_0^{\pi} d\theta \sin\theta \\
&\quad \times \sum_{j,m} \left[\beta_j \beta_m^* \exp[-ik_0 \hat{\mathbf{k}} \cdot (\mathbf{r}_j - \mathbf{r}_m)] \right].
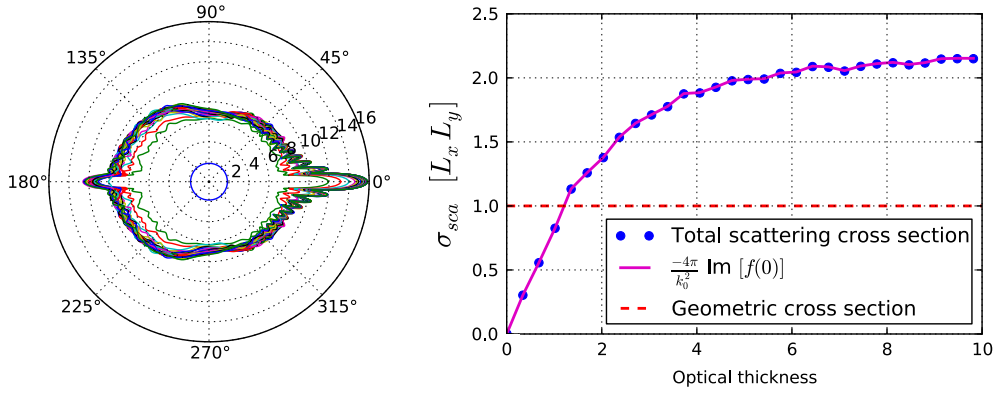\end{aligned}
\tag{31}
$$

Figure 2. Illustration of the optical theorem. Left: the scattered intensity integrated along ϕ, i.e. $g(\theta) = \int_0^{2\pi} d\phi |f(\theta, \phi)|^2$, is shown for resonant light $\Delta_0 = 0$ and a slab geometry with a uniform density distribution. The number of atomic scatterers is varied between 1 and 5000 (from inside to outside curves). The transverse size of the slab is $L_{x,y} = 80/k_0$ and the longitudinal size is varied such that $L_z = (20/k_0)N/5000$. This procedure allows us to vary the optical thickness $b_0 = 4\pi N/(k_0^2 L_x L_y)$ between 3×10^{-3} and 10 while maintaining the atomic density constant. We would like to insist on the fact that the optical thickness is computed for the scattering of a scalar field which leads to an unusual resonant cross-section for light $\sigma_0 = \lambda^2/\pi$ (different from the well-known resonant cross-section $\sigma_0 = 3\lambda^2/(2\pi)$ for vectorial light). The incident field is coming from the left and the intensity is plotted in log-scale. In addition to the forward Mie-like lobe, a lobe is also observed in the backward direction which we attribute to light reflection due to the sharp variation of optical index when the light hits the slab. Right: the blue circles represent the total scattering cross-section obtained by integrating the emission diagram over θ and ϕ, i.e. $\sigma_{sca} = 1/k_0^2 \times \int_0^\pi d\theta \sin(\theta)g(\theta)$. In our microscopic model, there is no absorption so that $\sigma_{abs} = 0$, leading to $\sigma_{ext} = \sigma_{sca}$. The optical theorem Equation (29) can thus be written as $\sigma_{sca} = -(4\pi/k_0^2)\text{Im}[f(0)]$, which is plotted in magenta. The good agreement between the two curves illustrates the validity of the optical theorem. (The color version of this figure is included in the online version of the journal.)

Consequently, using Equations (18) and (19), the average force along the z-axis reads:

$$F_z = \frac{\hbar k_0 \Gamma}{4\pi N} \int_0^{2\pi} d\phi \int_0^\pi d\theta \sin\theta(1 - \cos\theta)$$
$$\times \sum_{j,m=1}^N \left(\beta_j \beta_m^* \exp[-i\mathbf{k} \cdot (\mathbf{r}_j - \mathbf{r}_m)] \right). \quad (32)$$

We observe from Equation (32) that the average radiation pressure force is not merely proportional to the excitation probability, i.e. $\sum_j |\beta_j|^2$, but it is the result of an interference between the different atomic dipoles β_j. For this reason a measurement of the force captures the coherence properties of the scattering process as well as the detection of the light intensity. To make this point more explicit, using Equation (9), it is possible to write the force as

$$F_z = \frac{r^2}{Nc} \int_0^{2\pi} d\phi \int_0^\pi d\theta \sin\theta(1 - \cos\theta)I_s(\theta, \phi), \quad (33)$$

where the scattered far-field intensity is $I_s(\theta, \phi) = 2c\epsilon_0 |E_s(\theta, \phi)|^2$. This highlights the fact that the radiation pressure force, that pushes the atoms along the direction of the incident beam, is proportional to the net radiation flux of the scattered intensity.

In the case of an isotropic emission (e.g. single-atom case, or cloud much smaller than the wavelength), the scattered intensity I_s is independent of the angle and we get $F_z = (4\pi r^2/(Nc))I_s$: the direct proportionality between scattered power and radiation pressure force is recovered.

The cooperative effect of light scattering in such small samples is then encoded in the total scattered intensity I_s. In the case of superradiant scattering for larger samples, a pronounced emission into the forward direction decreases the radiation force, as observed for example in [8].

6. Scaling of the scattering cross-section

In this section we are interested in understanding how the scattering cross-section scales with the parameters of the system. We consider the case of a slab with uniform density distribution. The slab contains N atoms and its size along the x, y, z axes is denoted by L_x, L_y, L_z respectively. The numerical simulations presented in Figure 3 show how the scattering cross-section depends on the optical thickness of the cloud $b_0 = 4\pi N/(k_0^2 L_x L_y)$. For dilute clouds of atoms we find:

$$\sigma_{sca} = 2.15 \times L_x L_y \left[1 - \exp\left(-\frac{b_0}{2.15}\right) \right]. \quad (34)$$

When the slab is optically thick, i.e. $b_0 \gg 1$, we observe that the cross-section appears to approach $2 \times L_x L_y$. This factor of two corresponds to the well-known 'extinction paradox' [25,26] for which the extinction cross-section is twice as large as the one predicted by geometrical optics due to the diffraction contribution. The residual deviations from the factor of 2 between the scattering and geometrical cross-sections might be associated with a still moderate size of our sample [27], or to dipole blockade effects [28,29]. For spherical dielectric spheres, σ_{ext} shows an oscillatory behavior
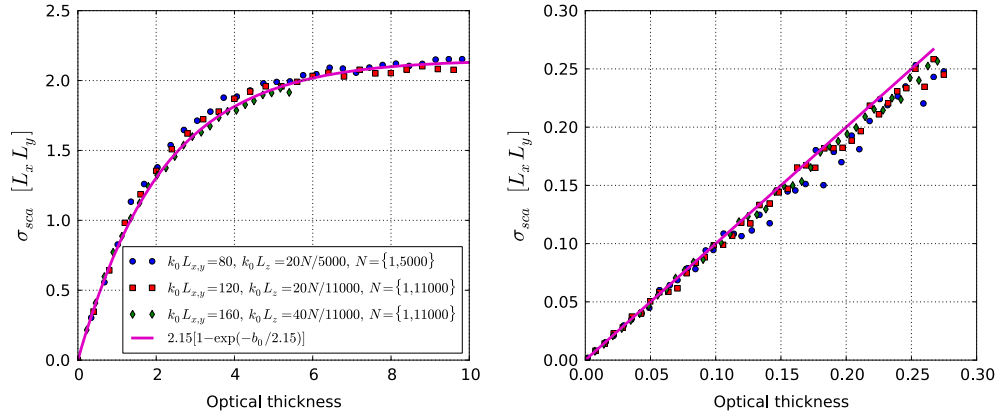
Figure 3. Scaling of the scattering cross-section. Left plot: following the same procedure as the one described in Figure 2, we compute the scattering cross-sections for different slab geometries. The results are shown in a scatter plot with different colors. The parameters of the simulations are reported in the legend of the figure. By fitting the data, constraining the slope in the limit $b_0 \to 0$ (right plot), we obtain a scattering cross-section that scales with the optical thickness b_0 of the slab according to Equation (34) (magenta full line). (The color version of this figure is included in the online version of the journal.)

around $2\sigma_{\mathrm{geo}}$ ($\sigma_{\mathrm{geo}} = L_x L_y$ for our square geometry), which is damped for increasing sizes of the sphere [30,31]. When $b_0 \ll 1$ the scattering cross-section can be written as $\sigma_{\mathrm{sca}} = (L_x L_y) b_0 = N\sigma_0$, where $\sigma_0 = \lambda^2/\pi$ is the resonant scattering cross-section for a single atom in the scalar wave description (it differs from the well-known cross-section for vectorial light $\sigma_0 = 3\lambda^2/(2\pi)$). In this limit, the interpretation is clear: at low optical thickness the cooperative effects are negligible and the scattering of light is given by the response of N independent atoms. We refer the reader to [32] for a study of the areal scaling of the light scattering by varying the size of a dense, cold atomic cloud.

Before concluding, we would like to underline the importance of the role of diffraction. Since we are using a microscopic description of the system, diffraction effects for the scattered field are already included in our model. However, free propagation of the incident field needs to be added for a fully consistent description. In this respect, the incident plane wave considered so far in the paper is a peculiar case. We will focus on these aspects in forthcoming studies to precisely understand the role of diffraction. This will naturally lead us to compare our coherent microscopic model of coupled dipoles to stochastic incoherent models commonly used to describe photon propagation in random media. Understanding coherent light propagation in disordered resonant scatterers is of prime importance for both the atomic physics and the waves in complex media communities.

7. Conclusion

We here discussed the superradiant emission of a cloud of cold atoms, when the interference of the waves radiated by the atomic dipoles builds up a coherent emission. Despite the fact that the simple relation between absorbed photons

and radiation pressure force existing in the single-atom case was lost, the optical theorem allowed one to recover a simple relation between the total scattered intensity and the displacement of the cloud center-of-mass. The measure of the force of the center of mass of the atomic cloud contains (partial) information on the scattered intensity, even for large values of optical thickness of the cloud. We have computed the total scattering cross-section which approaches a value close to twice the geometrical cross-section of the sample, in line with the well-known extinction paradox. Finally, understanding the role of diffraction paves the way for further studies to compare our coherent microscopic model to well-established stochastic incoherent models describing photon propagation in random media.

Acknowledgements

References

[1] Dicke, R.H. *Phys. Rev.* **1954**, *93*, 99–110.
[2] Friedberg, R.; Hartman, S.R.; Manassah, J.T. *Phys. Rep.* **1973**, *7*, 101–179.
[3] Keaveney, J.; Sargsyan, A.; Krohn, U.; Hughes, I.G.; Sarkisyan, D.; Adams, C.S. *Phys. Rev. Lett.* **2012**, *108*, 173601.
[4] Bachelard, R.; Courteille, Ph. W; Kaiser, R.; Piovella, N. *Europhys. Lett.* **2012**, *97*, 14004.
[5] Bienaimé, T.; Piovella, N.; Kaiser, R. *Phys. Rev. Lett.* **2012**, *108*, 123602.
[6] Morice, O.; Castin, Y.; Dalibard, J. *Phys. Rev. A* **1995**, *51*, 3896–3901.
[7] Courteille, Ph.W.; Bux, S.; Lucioni, E.; Lauber, K.; Bienaimé, T.; Kaiser, R.; Piovella, N. *Eur. Phys. J. D* **2010**, *58*, 69–73.

[8] Bienaimé, T.; Bux, S.; Lucioni, E.; Courteille, Ph.W.; Piovella, N.; Kaiser, R. *Phys. Rev. Lett.* **2010**, *104*, 183602.

[9] Campbell, G.K.; Leanhardt, A.E.; Mun, J.; Boyd, M.; Streed, E.W.; Ketterle, W.; Pritchard, D.E. *Phys. Rev. Lett.* **2005**, *94*, 170403.

[10] Bachelard, R.; Bender, H.; Courteille, Ph. W; Piovella, N.; Stehle, C.; Zimmermann, C.; Slama, S. *Phys. Rev. A* **2012**, *86*, 043605.

[11] Scully, M.O.; Fry, E.; Ooi, C.H.R.; Wodkiewicz, K. *Phys. Rev. Lett.* **2006**, *96*, 010501.

[12] Svidzinsky, A.A.; Chang, J.T.; Scully, M.O. *Phys. Rev. Lett.* **2008**, *100*, 160504.

[13] Bachelard, R.; Piovella, N.; Courteille, Ph.W. *Phys. Rev. A* **2011**, *84*, 013821.

[14] Bienaimé, T.; Petruzzo, M.; Bigerni, D.; Piovella, N.; Kaiser, R. *J. Mod. Opt.* **2011**, *58*, 1942–1950.

[15] Svidzinsky, A.A.; Chang, J.T.; Scully, M.O. *Phys. Rev. A* **2010**, *81*, 053821.

[16] Scully, M.O.; Svidzinsky, A.A. *Phys. Lett. A* **2009**, *373*, 1283–1286.

[17] Scully, M.O.; Svidzinsky, A.A. *Science* **2010**, *328*, 1239–1241.

[18] Röhlsberger, R.; Schlage, K.; Sahoo, B.; Couet, S.; Rüffer, R. *Science* **2010**, *328*, 1248–1251.

[19] Prasad, S.; Glauber, R.J. *Phys. Rev. A* **2010**, *82*, 063805.

[20] Bender, H.; Stehle, C.; Slama, S.; Kaiser, R.; Piovella, N.; Zimmermann, C.; Courteille, Ph.W. *Phys. Rev. A* **2010**, *82*, 011404.

[21] Piovella, N.; Bachelard, R.; Courteille, Ph.W. *J. Plasma Phys*. **2013**, 413–419 [also available on Cambridge Journals Online doi:10.1017/S0022377813000275].

[22] Gordon, J.P.; Ashkin, A. *Phys. Rev. A* **1980**, *21*, 1606–1617.

[23] van Albada, M.P.; Lagendijk, A. *Phys. Rev. Lett.* **1985**, *55*, 2692–2695.

[24] Wolf, P.-E.; Maret, G. *Phys. Rev. Lett.* **1985**, *55*, 2696–2699.

[25] Van de Hulst, H.C. *Light Scattering by Small Particles*; Dover: New York, 1981.

[26] Bohren, C.F.; Huffman, D.R. *Absorption and Scattering of Light by Small Particles*; Wiley: New York, 1983; pp 107–111.

[27] Chomaz, L.; Corman, L.; Yefsah, T.; Desbuquois, R.; Dalibard, J. *New J. Phys.* **2012**, *14*, 055001.

[28] Ott, J.R.; Wubs, M.; Lodahl, P.; Mortensen, N.A.; Kaiser, R. *Phys. Rev. A* **2013**, *87*, 061801(R).

[29] Bienaimé, T.; Bachelard, R.; Courteille, Ph.W.; Piovella, N.; Kaiser, R. *Fortschr. Phys.* **2013**, *61*, 377–392.

[30] Kargl, S.G.; Marston, P.L. *J. Acoust. Soc. Am.* **1990**, *88*, 1103–1113.

[31] Berg, M.J.; Sorensen, C.M.; Chakrabarti, A. *J. Quant. Spectrosc. Radiat. Transfer* **2011**, *112*, 1170–1181.

[32] Sokolov, I.M.; Kuraptsev, A.S.; Kupriyanov, D.V.; Havey, M.D.; Balik, S. *J. Mod. Opt.* **2013**, *60*, 50–56.